



Research article

PCDD/F adsorption enhancement over nitrogen-doped biochar: A DFT-D study

Shijian Xiong^a, Minghui Tang^{a,*}, Wenqian Jiang^a, Jiamin Ding^b, Juan Qiu^b, Shengyong Lu^{a,b}, Jianhua Yan^a^a State Key Laboratory of Clean Energy Utilization, Zhejiang University, Hangzhou, 310027, PR China^b Research Institute of Zhejiang University-Taizhou, Taizhou, 318012, Zhejiang, China

ARTICLE INFO

Handling Editor: Raf Dewil

Keywords:

2,3,4,7,8-Pentachlorodibenzo-p-furan
N-doping
Adsorption
Biochar
Density functional theory

ABSTRACT

Polychlorinated dibenzo-p-dioxin/furans (PCDD/F) have a great threat to the environment and human health, resulting in controlling PCDD/F emissions to regulation far important for emission source. Considering 2,3,4,7,8-pentachlorodibenzo-p-furan (PeCDF) identified as the most contributor to international toxic equivalent, 2,3,4,7,8-PeCDF can be considered as the target molecule for the adsorption of PCDD/F emission from industries. With the aim to in-depth elucidate how different types of nitrogen (N) species enhance 2,3,4,7,8-PeCDF on the biochar and guide the specific carbon materials design for industries, systematic computational investigations by density functional theory calculations were conducted. The results indicate pristine biochar intrinsically interacts with 2,3,4,7,8-PeCDF by π - π electron donor and acceptor (EDA) interaction, six-membered carbon rings of PeCDF parallel to the biochar surface as the strongest adsorption configuration. Moreover, by comparison of adsorption energy ($-150.16 \text{ kJ mol}^{-1}$) and interaction distance (3.593 \AA) of pristine biochar, environment friendly N doping can enhance the adsorption of 2,3,4,7,8-PeCDF on biochar. Compared with graphitic N doping and pyridinic N doping, pyrrolic N doping biochar presents the strongest interaction toward 2,3,4,7,8-PeCDF molecule due to the highest adsorption energy ($-155.56 \text{ kJ mol}^{-1}$) and shortest interaction distance (3.532 \AA). Specially, the enhancing adsorption of PeCDF over N doped biochar attributes to the enhancing π - π electron EDA interaction and electrostatic interaction. In addition, the effect of N doping species on PeCDF adsorbed on the biochar is more than that of N doping content. Specially, the adsorption capacity of N doping biochar for PCDD/F can be improved by adding pyrrolic N group most efficiently. Furthermore, pyrrolic N and pyridinic N doping result in the entropy increase, and electrons transform from pyrrolic N and pyridinic N doped biochar to 2,3,4,7,8-PeCDF molecule. A complete understanding of the research would supply crucial information for applying N-doped biochar to effectively remove PCDD/F for industries.

1. Introduction

Polychlorinated dibenzo-p-dioxin and dibenzofurans (PCDD/F) are concerned with persistent organic pollutants due to extremely toxic and high carcinogenicity (Schechter, 2013). As a result, PCDD/F has a great threat to the environment and human health (Kulkarni et al., 2008). Generally, PCDD/F is a highly toxic persistent organic pollutant from industrial manufacture (cement/power production), waste incineration, and biomass incineration et al. (Huang et al., 2022). Therefore, controlling PCDD/F emissions to regulation is far more important for emission sources. Recently, as for the removal of PCDD/F from industrial manufacture, the adsorption technique to remove PCDD/F

emissions has attracted significant interest. Developing effective and cost materials to remove dioxins is now in urgent need. Tailored zeolites (Jäger et al., 2004), ZnO nanowires imidazolium-based ionic liquid (Pan et al., 2013), activated carbon (Atkinson et al., 2015; Ottaviani et al., 2011), graphene sheets (Kang, 2005; Zhang et al., 2014), and carbon nanotubes (Fagan et al., 2007; Long and Yang, 2001) have been studied to adsorb PCDD/F in experimental or theoretical fields. Modified activated carbon, graphene sheets, and carbon nanotubes are classified into carbon materials. Carbon materials show excellent adsorption ability and enhance interaction between tetrachlorodibenzo-p-dioxin (TCDD) and carbon materials, which was proven by the density functional theory (DFT). Overall, carbon material adsorption (Chang et al., 2009) has

* Corresponding author.

E-mail address: lytmh1214@zju.edu.cn (M. Tang).<https://doi.org/10.1016/j.jenvman.2023.118611>

Received 5 May 2023; Received in revised form 28 June 2023; Accepted 10 July 2023

Available online 13 July 2023

0301-4797/© 2023 Elsevier Ltd. All rights reserved.

been regarded as the most popular method to remove PCDD/F emissions due to the advantages of the high removal efficiency (>90%) and acceptable cost.

To develop carbon materials with excellent adsorption performance, metals atom doped has been constructed to enhance the interaction between TCDD and carbon materials in theoretical aspects, which includes Ni-doped boron nitride nanotubes (Wang et al., 2017b), Ni/Cu-doped graphene, Ca/Ti/S/Se-doped phosphorene (Zhang et al., 2017), Ti/Ag-doped graphene (Zhang et al., 2014). Metals atom doping can effectively improve adsorption ability towards the TCDD molecule due to the enhancing electronic transport capability of carbon materials. However, for the synthesis of metals doping carbon materials, the second pollution and high cost cannot be neglected in theory. In addition, in experiment aspects, Fe(NO₃)₃ (Zhao et al., 2015), sulfur-doped, bromine-doped active carbon (Atkinson et al., 2015), and carbamide modification (Zhan et al., 2021) have been proved to improve adsorption efficiency. However, chemical activation by Fe(NO₃)₃ H₂SO₄, NaOH, and KOH consumes massive acids or alkalis and is relatively not safe and ecologically harmful for applications. Therefore, an effective green carbon material with chemical functional groups is needed up to now.

Nowadays, nitrogen doping biochar is considered a promising adsorbent for organic pollutants from incineration among carbon material due to its environmentally friendly and effective adsorption (Wan et al., 2020). Volatile organic compounds (VOCs) have been proven to be absorbed in nitrogen doping biochar effectively (585 mg/g) (Lu et al., 2021). Moreover, as for the adsorption of SO₂ (Qu et al., 2018a), phenanthrene (Wang et al., 2020), and methanol (Ma et al., 2019), the effect of nitrogen doping has been reported. N doping can not only enhance the interaction between target pollutants and the surface but also increase the adsorption capacity. As for the PCDD/F adsorption on carbon materials in the experimental field, most research (Qiu et al., 2018; Shen and Zhang, 2019) focuses on the pore structure of activated carbon by Alkali metal activation and microwave radiation, due to the significant impact of pore structure (Karademir et al., 2004; Li et al., 2016). Though in the experimental field, active carbon modified by urea (Zhan et al., 2021) has been conducted to adsorb PCDD/F, by modifying the N functional group on activated carbon surface. However, no research reports the adsorption of PCDD/F on nitrogen doping biochar in theoretical field, resulting in the lack of in-depth understanding for the adsorption between PCDD/F and biochar. Therefore, environmental nitrogen doping biochar with the high removal efficiency is lacking.

Among two hundred and ten PCDD/F congeners, 2,3,7,8-TCDD is the most toxic one. Due to the centrosymmetric and axisymmetric structure, the 2,3,7,8-TCDD molecule can be favored in theoretical aspects. All previous studies (Fagan et al., 2007; Pan et al., 2013; Zhang et al., 2014, 2017) have adopted the 2,3,7,8-TCDD molecule as a substitution to investigate the adsorption of PCDD/F on the surface, owing to 2,3,7,8-TCDD as the most toxic congener. However, according to the PCDD/F emission inventory in China (Huang et al., 2022), PCDD/F emissions are mainly from cement production, coke production, and waste incineration (including municipal, industrial, and medical waste). Among PCDD/F congeners from the main emission inventories (industries), 2,3,4,7,8-pentachlorodibenzo-p-furan (PeCDF) (Fu et al., 2022; Lin et al., 2014; Ryu et al., 2005) has been identified as the most contributor (>30%) (Zhang et al., 2022) to international toxic equivalent (I-TEQ), with great threat to ecosystems (Zhang et al., 2023) and human health (Yang et al., 2022). On the other hand, the 2,3,7,8-TCDD contributes less than 5% to I-TEQ among 2,3,7,8-substituted congeners. Therefore, 2,3,4,7,8-PeCDF can be considered the target molecule for the adsorption of PCDD/F. For aromatic pollutants (naphthalene (Wang et al., 2017a) and phenanthrene (Wang et al., 2020)) on graphene-like biochar surfaces, previous studies have reported π - π electron donor and acceptor (EDA) interaction was essential, compared with Lewis acid-base interactions (Li et al., 2019) and hydrogen bonding (Yang et al., 2017). Perdew-Wang functional within generalized gradient approximation has been widely adopted to accurately describe the

exchange-correlation energy for 2,3,7,8-TCDD molecule over surface. In addition, the dispersion effect for the conjugate system with the π - π EDA interaction was neglected for 2,3,7,8-TCDD molecules and surfaces (Izadmehri et al., 2017; Pan et al., 2013; Qian et al., 2011; Wang et al., 2017b; Zhang et al., 2014). Owing to the PeCDF-biochar system as weakly bound complexes, the van der Waals correction must be adopted to obtain exact calculation results. Up to now, no report about 2,3,4,7,8-PeCDF adsorbed on biochar can be found. In addition, the specific N functional group doping biochar with most strong interaction with PCDD/F can guide the design of biochar with excellent adsorption capacity.

In the present study, with the aim to in-depth elucidate how different types of N species enhance 2,3,4,7,8-PeCDF on the biochar and guide the specific carbon materials design for industries, systematic computational investigations by DFT-D calculations were conducted. First, the properties of 2,3,4,7,8-PeCDF and N-doped biochar were investigated to ensure lying configuration and standing configuration for the interaction between 2,3,4,7,8-PeCDF and pristine biochar. Moreover, the interactions between 2,3,4,7,8-PeCDF and N-doped biochar were compared by adsorption energy and interaction distance. In addition, the electronic properties and density of state were deeply calculated to reveal the electron transformation. The effect of N content was investigated to reveal the relationship between N content and adsorption energy. Furthermore, the effect of temperature and pressure on the PeCDF adsorbed in the biochar was investigated. A complete understanding of the research would supply crucial information for applying N-doped biochar to effectively remove PCDD/F for industries.

2. Computational details

2.1. Calculation setting

The adsorption between biochar material and PeCDF molecule was studied with the density functional theory (DFT) method. Based on the previous study (Kong and Chen, 2013; Wang et al., 2020), pristine graphene was considered as the model surface. Considering the π - π EDA interaction of the benzene ring, van der Waals interaction is introduced into the calculation system according to density functional theory based on dispersion correction (DFT-D3) (Georgieva et al., 2017; Grimme et al., 2010; Hafner, 2008). The interactions between the valence electrons and the ionic core were described with the projected augmented wave (PAW) method (Enkovaara et al., 2010). The electronic exchange-correlation potential was treated using the generalized gradient approximation (GGA) function and Perdew-Burke-Ernzerhof (PBE) function (Wang et al., 2017b; Zhang et al., 2017). For the optimization of the 2,3,4,7,8-PeCDF molecule, the molecule was put into a space lattice of $a = b = c = 15 \text{ \AA}$, and the K points were set $5 \times 5 \times 5$. As shown in Fig. S3, the pristine or doped biochar contains 100 atoms. Therefore, the pristine or doped biochar is placed inside a large cell of $17.2 \text{ \AA} \times 17.2 \text{ \AA} \times 25 \text{ \AA}$ to neglect the interaction between biochar in the bundle safely. The Brillouin zone was sampled with a Monkhorst-Pack k-point grid of $2 \times 2 \times 1$ for pristine or doped biochar. To determine the optimum adsorption sites and geometries, the 2,3,4,7,8-PeCDF molecule and each biochar surface were allowed to relax unconstrainedly until residual forces on all atoms had reached 0.03 eV \AA^{-1} . All calculations were carried out in Vienna Ab-initio Simulation Package (VASP) version 5.4.4. After optimizing the molecule, biochar, and molecule-biochar structure, the change of total energy is less than 10^{-7} eV , which meets the standard of convergence (Fang et al., 2020). The highest occupied molecular orbital (HOMO) and lowest unoccupied molecular orbital (LUMO) were calculated to describe the characteristic of the 2,3,4,7,8-PeCDF molecule. The figures of electronic properties were draw by VESTA3 (Momma and Izumi, 2011).

2.2. Calculation analyses

In order to acquire different aspects of calculation results, the following aspects are raised.

2.2.1. Adsorption strength of PeCDF

The adsorption energy (E_{ad}), indicating the intensity of interaction between a PeCDF molecule and biochar, is derived according to the following equation (1):

$$E_{ad} = E_{surface+PeCDF} - (E_{surface} + E_{PeCDF}) \quad (1)$$

where $E_{surface+PeCDF}$, E_{PeCDF} , and $E_{surface}$ represent the total energy of the PeCDF-biochar system, the energy of the PeCDF molecule, and the energy of the pristine, N doped biochar, respectively. A negative E_{ad} value corresponds to stable adsorption, and the more negative the E_{ad} is, the more stable the adsorption will be.

The difference charge density was utilized to study the change in charge density during adsorption, calculated by subtracting the charge density of the isolated PeCDF molecule (ρ_{PeCDF}) and the phosphorene surface ($\rho_{surface}$) from the total charge density of the system ($\rho_{PeCDF+surface}$), as shown in Equation (2):

$$\Delta\rho = \rho_{PeCDF+surface} - \rho_{PeCDF} - \rho_{surface} \quad (2)$$

The density of states (DOS) and partial density of states (PDOS) analysis can be effective methods of exploring the interactions between PeCDF molecules and N-doped biochar at the electronic level.

2.2.2. Effect of temperature and pressure on adsorption energies

To reflect how temperatures affect adsorption energies of PeCDF over N-doped biochar, Gibbs free energy is introduced to reflect adsorption energies. The definitions for Gibbs free energies are seen as follows (Hu et al., 2021; Yang et al., 2019):

$$G_{gas}(T) = E_{mole} + ZPE + RT - TS \quad (3)$$

$$G_{solid}(T) = E_{surface} + ZPE - TS \quad (4)$$

where $G_{gas}(T)/G_{solid}(T)$ are Gibbs free energies of gases/solids, respectively, $E_{mole}/E_{surface}$ is the ground-state energy of the molecule or surface, ZPE is zero-point energy correction, R is the gas constant (i.e. 8.314 J mol⁻¹.K⁻¹), T is the temperature, and S is the entropy computed from vibrational frequency calculations.

Then, to reflect how pressure affects adsorption energies of PeCDF over N-doped biochar, Gibbs free energies are introduced to adsorption energies.

$$G_{gas}(P) = E_{mole} + ZPE + RT^0P/P^0 - T^0S \quad (5)$$

$$G_{solid}(P) = E_{surface} + ZPE + RT^0P/P^0 - T^0S \quad (6)$$

The Gibbs adsorption energy is defined as follows (Yang et al., 2019):

$$G_{ad} = G_{surface+PeCDF} - (G_{surface} + G_{PeCDF}) \quad (7)$$

where $G_{surface+PeCDF}$, G_{PeCDF} , and $G_{surface}$ represent the total energy of the PeCDF-biochar system, the energy of the PeCDF molecule, and the energy of the pristine, N doped biochar, respectively. The post-processing of the VASP calculated data and calculation of Gibbs free energy were conducted in the post-processing VASPKIT package (Wang et al., 2021).

3. Results and discussion

3.1. Structure of 2,3,4,7,8-PeCDF and N-doped biochar

3.1.1. Feature of 2,3,4,7,8-PeCDF

The optimized structure of 2,3,4,7,8-PeCDF molecules is shown in Fig. 1 (a). The parameters of bond length are exhibited in Table S1. Deduced from the difference in bond length of two carbon rings, the 2,3,4,7,8-PeCDF molecule presents inconsistent characteristic. According to the electrostatic potential of the 2,3,4,7,8-PeCDF molecule in Fig. 1 (b), the electrostatic potential of hydrogen is higher than that of an oxygen atom and chlorine atoms. As a result, two adsorption geometries of PeCDF standing on biochar with two hydrogen atoms (Fig. 1 (d)) and an oxygen atom (Fig. 1 (f)) must be considered. Owing to the uniform electrostatic potential, the configuration of PeCDF lying on biochar (Fig. 1 (g)) must be conducted. The LUMO and HOMO are -0.0837 eV and -0.2529 eV, respectively. Hence, the HOMO-LUMO gap is -0.1692 eV. The PeCDF molecule tends to receive electronics. In addition, as shown in Figs. S2(a) and (b), the LUMO and HOMO map of molecule presents inconsistency of chlorine atoms connected on two carbon rings. Therefore, two adsorption geometries of PeCDF standing on biochar with three chlorine atoms (Fig. 2 (c)) and two chlorine atoms (Fig. 1 (e)) must be considered. In summary, five configurations of PeCDF on biochar must be calculated, which is more than that of TCDD on graphene (Kang, 2005) or phosphorene (Zhang et al., 2017). Nevertheless, the results indicate the calculation of PeCDF adsorbed on biochar is harder than that of 2,3,7,8-TCDD on biochar.

3.1.2. Feature of N-doped biochar

Firstly, according to X-ray photoelectron spectroscopy spectra of N 1s of nitrogen (N) doped biochar, graphitic nitrogen, pyridinic nitrogen, and pyrrolic nitrogen were proven on the surface of N-doped biochar (Lu et al., 2021; Tang et al., 2020). Then, the pristine and N-doped biochar surfaces with graphitic nitrogen, pyridinic nitrogen, and pyrrolic nitrogen were constructed. The configurations of N functional groups in the biochar refer to Ma's work (Ma et al., 2019) and Qu's work (Qu et al., 2018a). Moreover, due to the diameter of PeCDF molecule (1.34 nm), the mesopores plays key role for the adsorption of PeCDF on graphene materials (Li et al., 2016) and carbon nanotubes (Zhou et al., 2015). N doped biochar contains many mesopores (Kasera et al., 2022; Liu et al., 2023), with potential to remove PCDD/F effectively. To investigate the electronic properties of the N-doped biochar surface, the charge density of pristine and N-doped biochar is illustrated in Fig. 2. As compared with the pristine surface (Fig. 2(a)), graphitic N, pyridinic N, and pyrrolic N doping all produce higher charge density and asymmetrical charge distribution. Moreover, the maximum charge density of the surface is the biochar with pyridinic N (0.668 e/Bohr³), followed by the biochar with pyrrolic N atom (0.606 e/Bohr³), the biochar with graphitic N atom (0.564 e/Bohr³), pristine biochar (0.316 e/Bohr³). The result implies that N doping increases the accumulation of electrons of the N atom. More specifically, the charge density of the N atom is two times that of the carbon atom on the graphitic N-doped biochar. Nevertheless, the N-doped biochar presents the potential to enhance the adsorption between PeCDF and biochar. The results are in accord with the experiment on nitrogen-doped biochar (Wan et al., 2020).

Moreover, to investigate the effect of N doping on the electronic properties, the electrostatic potential was analyzed. The changes in electrostatic potential can significantly influence the interaction between surface and molecules (Kong and Chen, 2013; Wheeler and Bloom, 2014). Fig. 2 (e)-(g) shows the electrostatic potential map of three N-doped biochar. Compared with the pristine surface (Fig. S3), N doping results in the enhancement or weakening of electrostatic potential within the biochar surface. Specially, for graphitic N-doped biochar, the electrostatic potential of the region near N atoms enhances. For the pyridinic N-doped surface, the red region can be observed around N atoms, suggesting negative electrostatic potential. The

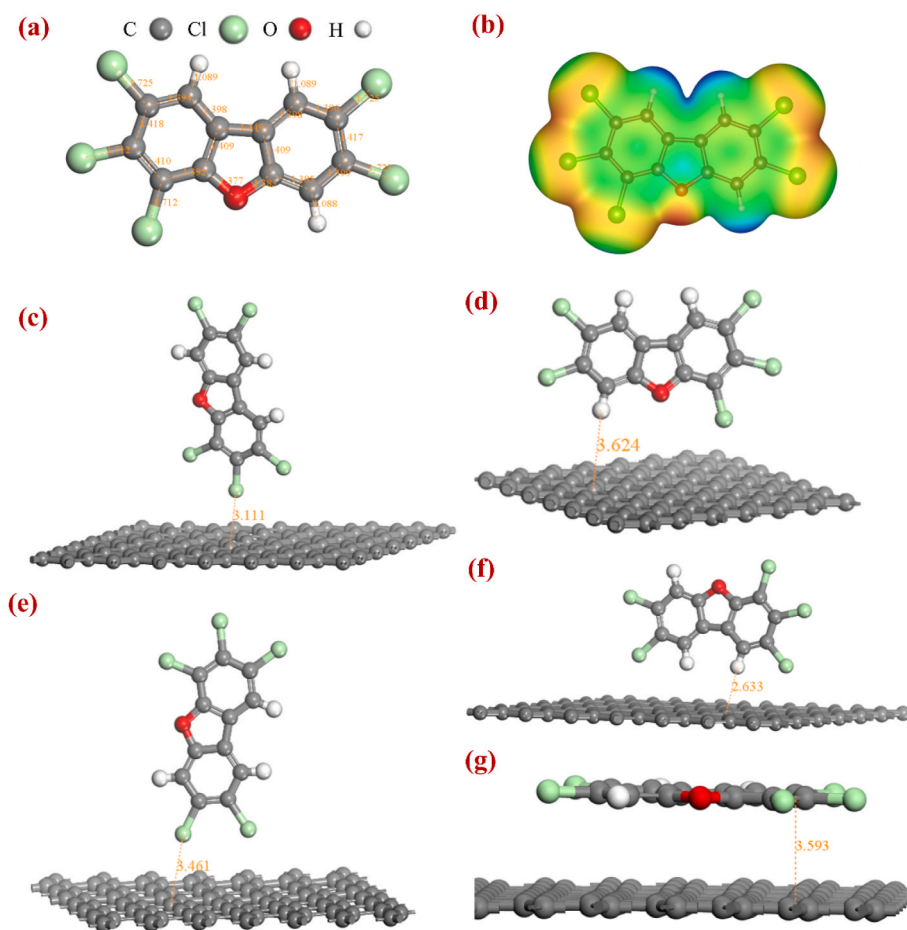


Fig. 1. Structure (a) and electrostatic potential (isosurface level = 0.002 e/Bohr³) (b) of 2,3,4,7,8-PeCDF molecule; optimized ball and stick models of PeCDF-biochar: (c) PeCDF standing on biochar with three chlorine atoms, (d) PeCDF standing on biochar with an oxygen atom, (e) PeCDF standing on biochar with two chlorine atoms, (f) PeCDF standing on biochar with two hydrogen atoms, (g) PeCDF lying on biochar. (The structural parameters are shown in Å).

outcome further indicates that pyridinic N can donor electrons for the biochar surface interacting with PeCDF. With regard to the pyrrolic N-doped surface, the blue region can be observed around the pyrrolic N-doped, suggesting strong positive electrostatic potential. This result indicates that hydrogen and pyrrolic N atoms can accept electrons for the biochar surface interacting with PeCDF. The above results are in accord with the previous study about N-doped carbon clusters (Qu et al., 2018b).

3.2. PeCDF adsorption on the N-doped biochar

For the adsorption of PeCDF on the pristine biochar, various possible adsorption geometries were considered, including the hexagonal ring of PeCDF parallel and perpendicular to the biochar surface with a chlorine site or oxygen site. Five stable adsorption configurations are presented in Fig. 1, denoted as (c), (d), (e), (f), and (g), and the adsorption energy of five configurations are shown in Table S2. For configuration (c), the two six-membered carbon rings of PeCDF are almost perpendicular to biochar with three Cl atoms close to the surface. The calculated E_{ad} value is $-91.55 \text{ kJ mol}^{-1}$ and the interaction distance is 3.111 Å. For configuration (d), the two six-membered carbon rings of PeCDF are almost perpendicular to biochar with two Cl atoms and close to the surface. The calculated E_{ad} value is $-77.98 \text{ kJ mol}^{-1}$ and the interaction distance is 3.461 Å. In addition, for configuration (f), the two six-membered carbon rings of TCDD are perpendicular to the biochar surface with two H atoms and two Cl atom close to the surface. This structure is energetically relative unfavorable with the E_{ad} value being $-88.59 \text{ kJ mol}^{-1}$. For configuration (d), the two six-membered carbon

rings of PeCDF are perpendicular to the biochar surface with a hydrogen atom, two Cl atoms, and an O atom close to the surface. The adsorption energy between the PeCDF molecule and biochar surface is $-81.40 \text{ kJ mol}^{-1}$ and the interaction distance is 3.624 Å. For the most stable configuration (g), the adsorption energy between PeCDF and pristine biochar is $-150.16 \text{ kJ mol}^{-1}$, and the interaction distance is 3.593 Å. Therefore, the adsorption energy of PeCDF lying on biochar is significantly higher than that of the other configuration. It is found that the two six-membered carbon rings of PeCDF parallel to the biochar surface are the strongest adsorption configuration. The high adsorption energy and short interaction distance for the complex of PeCDF on biochar surface indicate the strong physical adsorption of pristine biochar surface toward PeCDF via π - π EDA interaction. The result is consistent with the adsorption mechanism between metal doped black phosphorene or nanotubes and 2,3,7,8-TCDD (Zhang et al., 2017) and adsorption experiment of PCDD/F on graphite (Li et al., 2016). As for the calculation without dispersion correction in previous studies (Kang, 2005), the adsorption energy between 2,3,7,8-TCDD and biochar ranged from $-28.94 \text{ kJ mol}^{-1}$ to $-38.59 \text{ kJ mol}^{-1}$. The adsorption energy between PeCDF and biochar surface is significantly higher with near interaction distance. Therefore, the van der wall interaction plays an essential role in the adsorption between PeCDF and biochar surface. In addition, the previous studies of PCDD/F adsorption on different materials focus on the most stable adsorption configurations for different materials (Wang et al., 2017b; Zhang et al., 2014, 2017). Therefore, for PeCDF on N doping biochar, it is reasonable to only consider the configuration of biochar parallel to PeCDF.

Next, for the adsorption of PeCDF molecule on the N doped biochar,

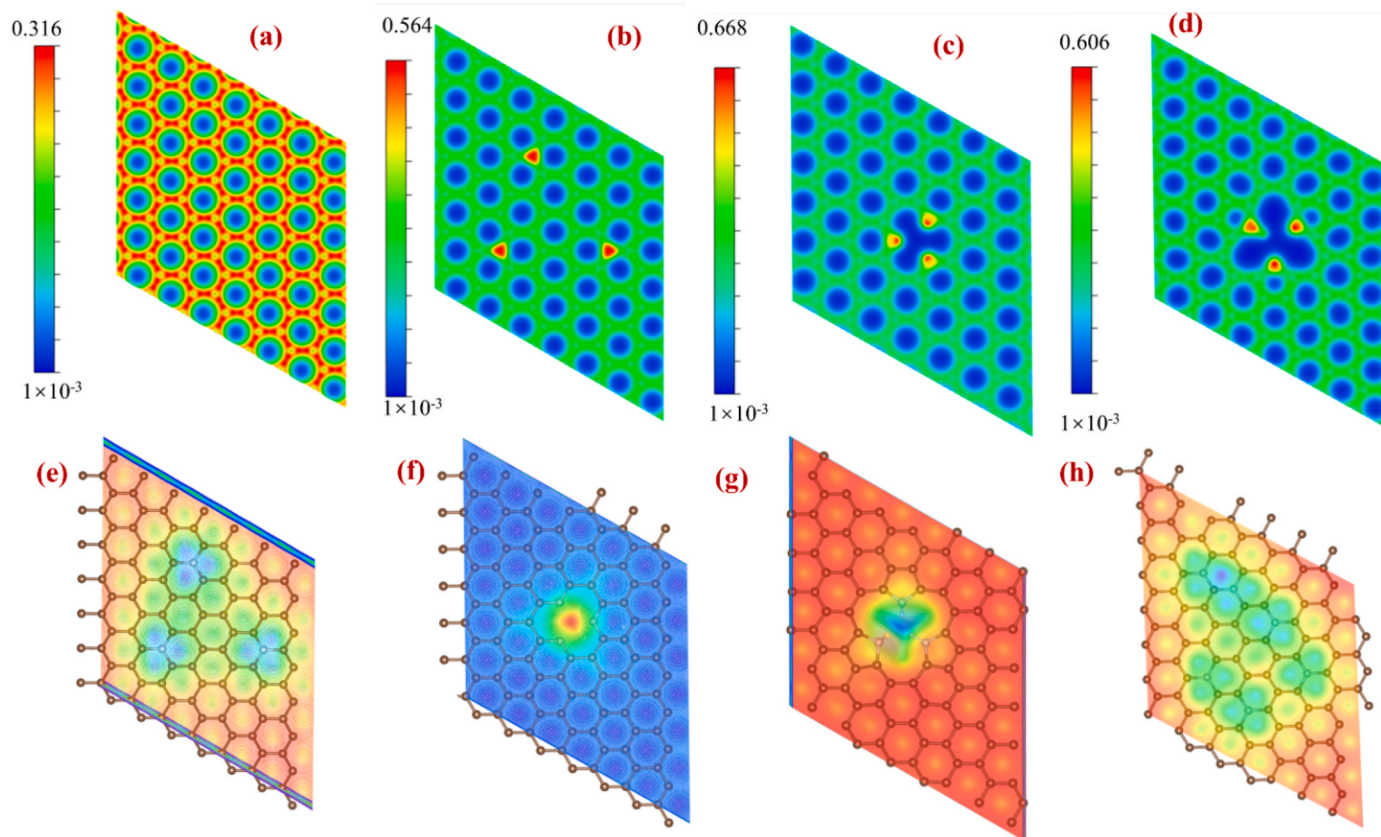


Fig. 2. The charge density of pristine and N-doped biochar. Biochar without any N atom (a), with graphitic N (b), with a pyridinic N (c), and with pyrrolic N atom (d); electrostatic potential of N-doped biochar. Biochar with graphitic N (e), with pyridinic N (f), and with pyrrolic N atoms (g), with 6% graphitic N (h) (isosurface level = 0.002 e/Bohr³).

the optimized physisorption complex of PeCDF on biochar surface with and without N doping is illustrated in Fig. 3. The adsorption energy between PeCDF and pristine and N doped biochar is presented in Table 1. For the graphitic N site adsorption, the adsorption energy increases to $-151.70 \text{ kJ mol}^{-1}$ from $-150.16 \text{ kJ mol}^{-1}$ of pristine biochar. Moreover, the adsorption energy is $-155.19 \text{ kJ mol}^{-1}$ and $-155.56 \text{ kJ mol}^{-1}$ for pyridinic N and pyrrolic N site adsorption, respectively. Though, the adsorption energy of N-doped biochar is only 1–5 kJ/mol lower than that of the biochar without any N atom. Due to the change of total energy is less than 10^{-7} eV , errors caused by calculation principles are less than 10^{-5} kJ/mol . Therefore, the change of adsorption energy is credible to supply that the N-doped biochar is superior to adsorbing PeCDF. It is found that N doping enhances the adsorption behavior of

Table 1

Adsorption energy between PeCDF and pristine and N doped biochar.

Species	$E_{\text{ad}} = E_{\text{surface + PeCDF}} - (E_{\text{surface}} + E_{\text{PeCDF}})$			
	$E_{\text{surface + PeCDF}}$ (eV)	E_{surface} (eV)	E_{PeCDF} (eV)	E_{ads} ($\text{kJ}\cdot\text{mol}^{-1}$)
Graphite	-1046.26	-908.22	-136.47	-150.16
Graphitic-N	-1040.99	-902.94	-136.47	-151.70
Pyridinic-N	-1030.74	-892.65	-136.47	-155.19
Pyrrolic-N	-1021.23	-883.13	-136.47	-155.56
Graphitic-6N	-1034.75	-896.69	-136.47	-153.40

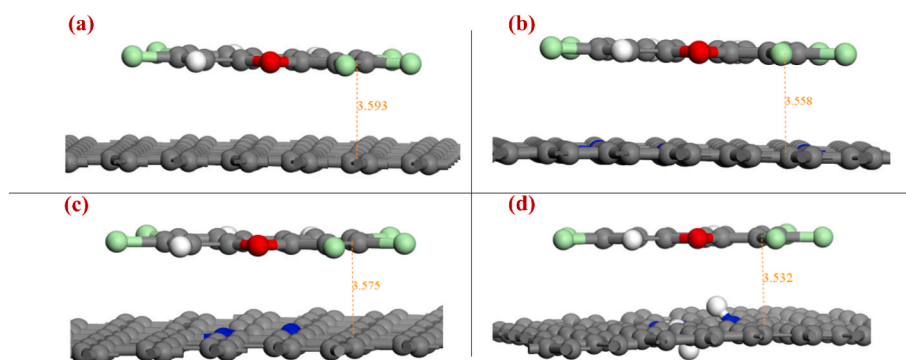


Fig. 3. Optimized physisorption complex of PeCDF on biochar surface with and without N doping. Biochar without any N atom (a), with graphitic N (b), with a pyridinic N (c), and with pyrrolic N atom (d).

PeCDF on the biochar. The results are consistent with the actual experimental result (Zhan et al., 2021) that the higher adsorption capacity of biochar with N functional group for PCDD/F, compared with active carbon. In addition, the interaction distance decreased from 3.593 Å to 3.558 Å, 3.575 Å, and 3.532 Å for graphitic N, pyridinic N, and pyrrolic N site adsorption, respectively. The smaller interaction distances imply the stronger interaction of PeCDF with N-doped biochar than the pristine biochar. The enhanced effect can attribute to the N doping increasing the charge-transfer ability of biochar to PeCDF. Finally, the pyrrolic N site presents the highest adsorption energy and shortest interaction distance among the three N-doped sites. The result indicates that the optimized most stable site is the pyrrolic N site.

3.3. Electronic properties

To understand the improved adsorption capability of the biochar toward PeCDF upon the N doping, the total electronic density of state (DOS) of the stable adsorption site is calculated. As shown in Fig. S4, the DOS of biochar near the Fermi level (energy = 0 eV) almost changed slightly after N doping. More specifically, the DOS of N-doped biochar is higher than that of pristine biochar in energy about -13 eV, 5 eV. Furthermore, the obvious difference in biochar can be found in the total DOS result after the adsorption of the PeCDF molecule. The result indicates a strong interaction between biochar and PeCDF molecule. As for PeCDF adsorbed on the pyridinic N-doped biochar, the DOS peak shifts to the left by 1 eV. In addition, among the three N-doped adsorption configurations of PeCDF, the pyrrolic N-doped biochar display the highest peak. The result is consistent with the analysis of adsorption energy.

The yellow isosurface represents the electron accumulation region and the cyan one represents the electron dissipation region. As shown in Fig. 4 (a) and (b), there were distinct charge transfers between N-doped biochar and 2,3,4,7,8-PeCDF molecule. Furthermore, the amount of charge transfer of N-doped biochar is more than that of pristine biochar. The results indicate that a strong interaction exists between the 2,3,4,7,8-PeCDF molecule and N-doped biochar. As for the PeCDF-graphitic N-doped biochar system (Fig. 4(b)), the isosurface near N atoms is yellow, and far from N atoms is cyan, considering that the isosurface near the carbon ring of the PeCDF molecule is yellow. The result indicates that the electrons of biochar far from N atoms transfer to the region near N atoms. With respect to the PeCDF-pyridinic N-doped biochar system (Fig. 4(c)), the isosurface near the oxygen ring of the PeCDF molecule is cyan and the isosurface on the outside of the PeCDF molecule is yellow. The result suggests that the electrons of the oxygen ring of the PeCDF molecule transfer to the region near N atoms. As for the PeCDF-pyrrolic N-doped biochar system, the isosurface near the oxygen ring of the PeCDF molecule is yellow and the isosurface on the outside of the PeCDF molecule is cyan (Fig. 4(d)). In addition, the isosurface area of the oxygen ring of the PeCDF molecule is the largest among PeCDF-graphitic N-doped biochar, PeCDF-pyridinic N-doped biochar, and PeCDF-pyrrolic N-doped biochar system. Therefore, the strongest interaction occurs between PeCDF and pyrrolic N-doped biochar. In addition, to compare the adsorption pattern of N doping, the top view for charge density difference of PeCDF-biochar system without N doping, with graphitic N with a pyridinic N, and with pyrrolic N atoms is shown in Fig. S5. The area of electron-electron transformation of PeCDF-biochar system with graphitic N doping is larger than that of PeCDF-biochar system without N doping. Hence, compared with the charge density difference of the PeCDF-biochar system without N doping, graphitic N doping enhances the electrostatic interaction. In addition, the pattern of electron-electron transformation of PeCDF-biochar systems with pyridinic N doping and pyrrolic N doping is similar with that of PeCDF-biochar system without N doping. Therefore, pyridinic N doping and pyrrolic N doping enhance π - π EDA interaction.

To quantitatively describe the electron-electron transformation from N doped biochar to PeCDF molecule, charge integral for (x,y) planes of

PeCDF-biochar system without any N atom, with graphitic N, with pyridinic N, and with pyrrolic N atoms are shown in Fig. 4 (e)–(f). Compared with the charge integral (x, y) of PeCDF-pristine biochar system, the charge integral (x,y) enhances at $z = 6$ Å for graphitic N doping. In addition, the charge integral (x,y) significant enhances at $z = 6$ Å and $z = 5$ Å for pyridinic N doping and with pyrrolic N doping, respectively. Generally, the pattern of electron transformation for the PeCDF molecule on the graphitic-N doped biochar is different from that for the PeCDF molecule on the pyridinic N or pyrrolic N doped biochar. Specially, the charge integral (x, y) of pyridinic N doping and with pyrrolic N doping system is higher than that of graphitic N doping at $z = 2$ – 6 Å.

3.4. Effect of N-doped content

To investigate the relationship between adsorption capacity and N content, the biochar with higher graphitic N content doping was constructed. According to the numbers of previous experiments (Cheng et al., 2023; Huang et al., 2023; Liang et al., 2022; Lin et al., 2023; Liu et al., 2023), the N content in biochar most ranges from 3% to 6%. The pore structure of biochar can be destroyed if the N content in biochar is too high (>8%), resulting in the low adsorption capacity for PCDD/F. Hence, the design of 3% and 6% N content doping is reasonable. The reasons for selecting graphitic N doping to analyze the effect of N doping content are the following: (1) the enhancing effect of adsorption between PeCDF and graphitic N doped biochar is in accord with that between PeCDF and pyridinic or pyrrolic N doped biochar; (2) the homogeneity of N doping on the surface can ensure by graphitic N rather than pyridinic or pyrrolic N doping. As shown in Fig. 2 (h), the electrostatic potential near graphitic N doping is higher than that near carbon atoms, and the pattern of 6% graphitic N doping is similar to that of 3% graphitic N doping. As the optimized PeCDF-6% graphitic N doped biochar is present in Fig. 5 (a), the adsorption energy is -153.40 kJ mol⁻¹ and the interaction distance is 3.516 Å. Hence, the adsorption energy increases by -1.54 kJ mol⁻¹ and the interaction distance decreases by 0.042 Å. The result indicates that PeCDF can be stronger absorbed on 6% graphitic N doped biochar by a shorter adsorption distance. Compared to the system with 3% graphitic N doped biochar, the results indicate higher N content contributes to more electron transformation in Fig. 5 (b). Moreover, the DOS of PeCDF on biochar surface with 6% N doping is shown in Fig. S6. The adsorption enhancement of 6% N doping can be observed in the view of molecular orbital composition. As shown in Fig. 5 (d), the adsorption energy has a near-perfect linear relationship with N content. The coefficient of determination is 0.999. The result indicates that higher N content contributes to higher adsorption capacity, similar with the adsorption of methanol adsorption over nitrogen-rich carbon (Ma et al., 2019). Especially, the adsorption energy of the PeCDF-biochar with 6% graphitic N content doping is smaller than that of PeCDF-biochar with 3% pyrrolic N content doping. The result indicates that the effect of N doping species on PeCDF adsorbed on the biochar is more than that of N doping content. Hence, the adsorption capacity of N doping biochar for PCDD/F can be improved by adding pyrrolic N group most efficiently.

3.5. Effect of temperature and pressure

To investigate the influence of temperature on the adsorption of PeCDF on biochar, adsorption Gibbs adsorption energy was calculated to present thermal vibrations. The temperature and pressure setting refers to the operating temperature of PCDD/F on N-doped biochar (Chen et al., 2020; Li et al., 2016; Zhan et al., 2021) and the operating pressure (Lv et al., 2021) of bag filter in industries. On the basis of Eqs (3)–(7), the results of Gibbs adsorption energy at different temperatures and different pressure are shown in Fig. 6. As shown in Fig. 6 (a), Gibbs adsorption energy of 2,3,4,7,8-PeCDF decreases with increasing temperature, indicating an exact trend. This trend is in accord with carbon

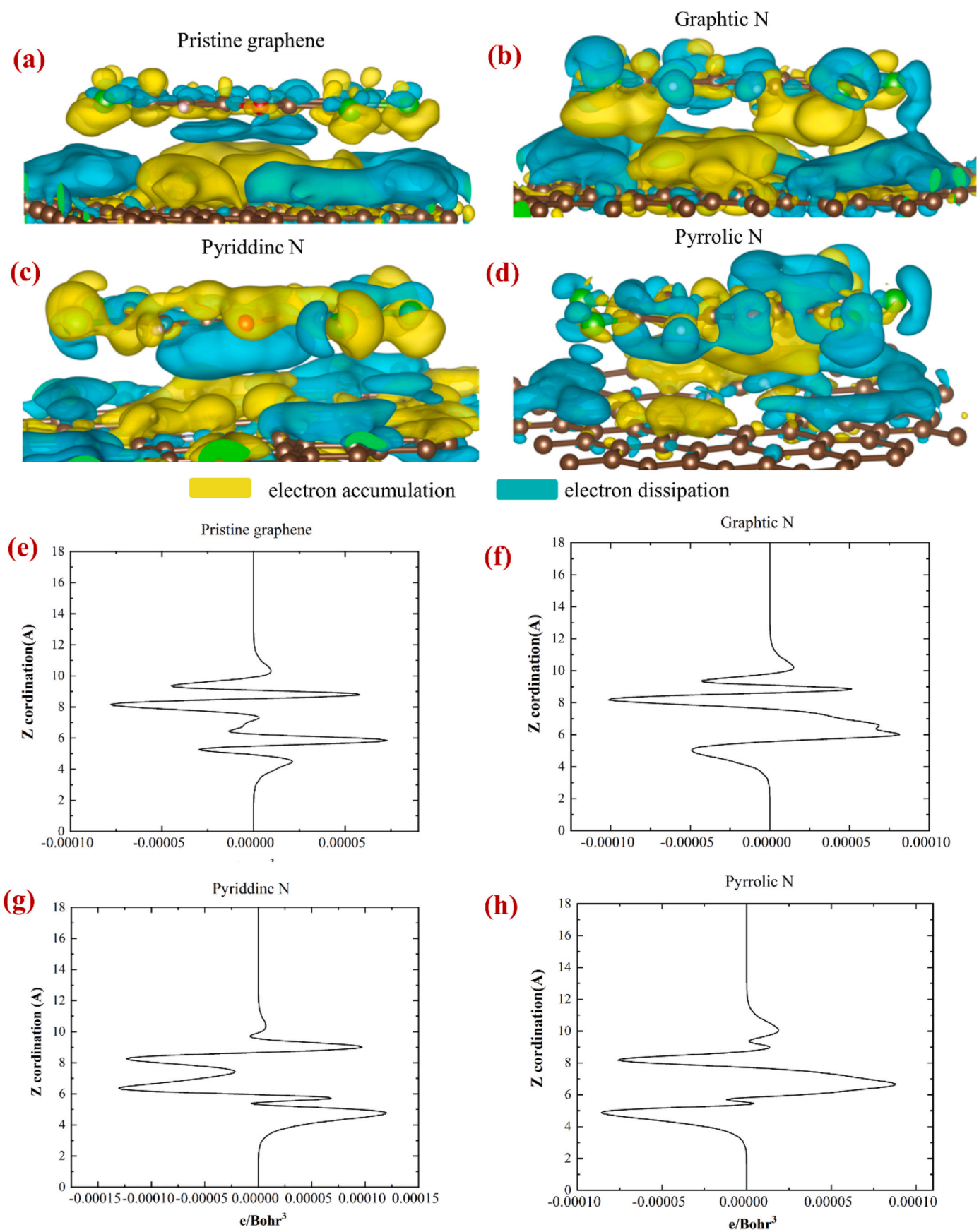


Fig. 4. Charge density difference of PeCDF-biochar system without any N atom (a), with graphitic N (b), with a pyridinic N (c), and with pyrrolic N atoms (d) (isosurface value: $5 \times 10^{-5} e/\text{Bohr}^3$); charge integral for (x,y) plane of PeCDF-biochar system without any N atom (e), with graphitic N (f), with pyridinic N (g), and with pyrrolic N atoms (h).

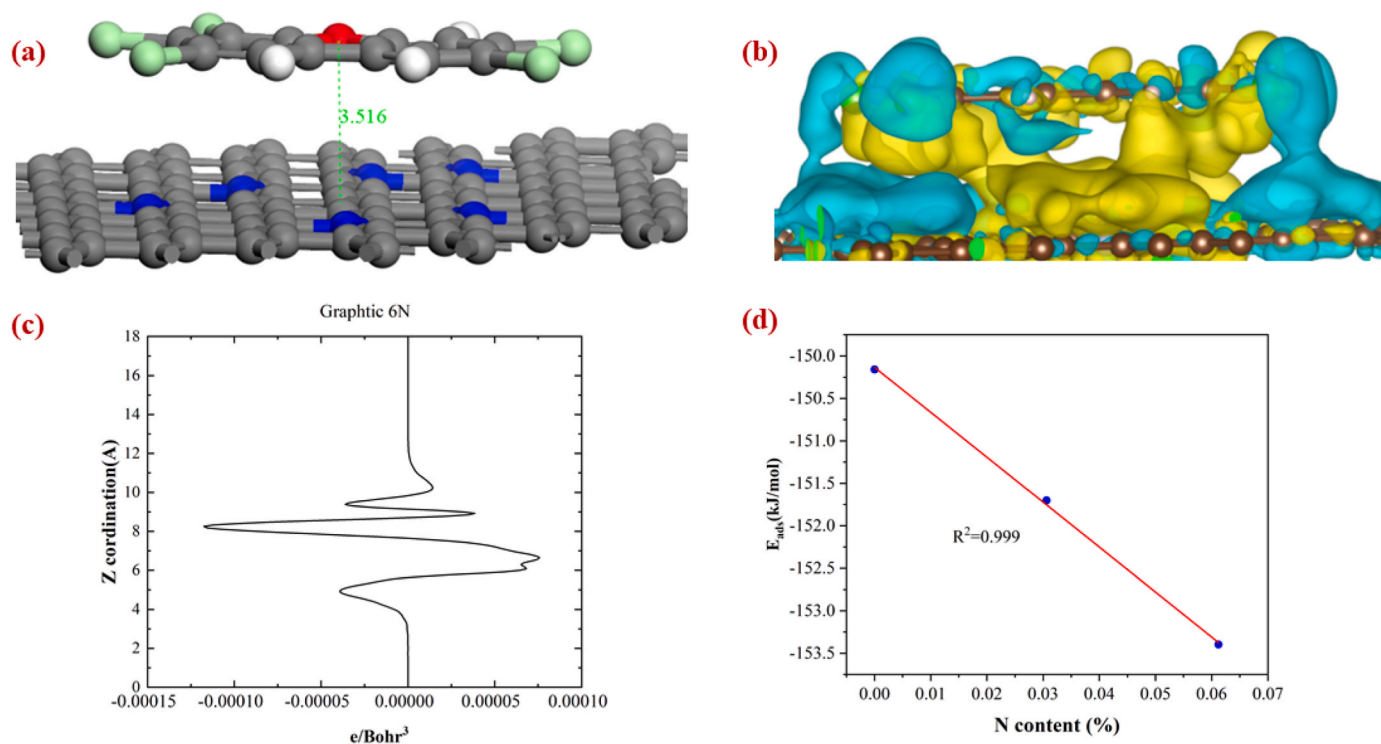


Fig. 5. Optimized configuration (a); difference charge density (isosurface value: $5 \times 10^{-5} \text{ e/Bohr}^3$) (b); charge integral for (x,y) plane of 2,3,4,7,8-PeCDF-6% N-doped biochar system (c); (d) relationship between adsorption energy and N content.

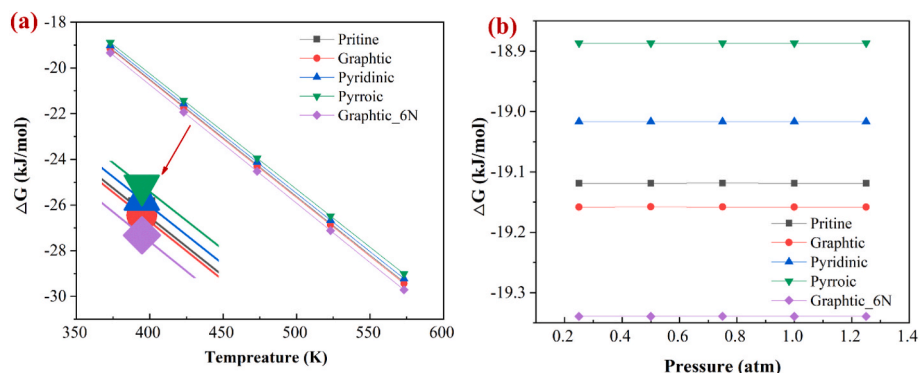


Fig. 6. Gibbs adsorption energies of 2,3,4,7,8-PeCDF over N-doped biochar at different temperatures (a) and different pressure (b).

dioxide over hexagonal boron nitride (Hu et al., 2021). Specially, the adsorption Gibbs adsorption energy of 2,3,4,7,8-PeCDF adsorbed on pyrrolic N doped biochar is higher than that adsorbed on the pristine surface, followed by pyridinic N doped biochar. The result indicates that the adsorption behavior of 2,3,4,7,8-PeCDF adsorbed on pyrrolic N and pyridinic N doped biochar results in the entropy increase of 2,3,4,7,8-PeCDF molecule. Therefore, overall, the 2,3,4,7,8-PeCDF molecule accepts electrons. In contrast to this result, the Gibbs adsorption energy of 2,3,4,7,8-PeCDF adsorbed on graphitic N doped biochar is lower than that adsorbed on a pristine surface. In addition, the Gibbs adsorption energy of 2,3,4,7,8-PeCDF adsorbed on 6% graphitic N doped biochar is significantly lower than that adsorbed on 3% graphitic N doped biochar. As a result, the adsorption behavior of 2,3,4,7,8-PeCDF adsorbed on graphitic N doped biochar results in the entropy decrease of the 2,3,4,7,8-PeCDF molecule. Furthermore, with more N atoms being doped in biochar, adsorption Gibbs free energy decreases. The result further proves the fact that high N doping content can enhance the adsorption of 2,3,4,7,8-PeCDF on biochar. Specially, the Gibbs free energies of 2,3,4,7,

8-PeCDF before and after adsorption for different temperatures were shown in Table S3. As the temperature increase, the Gibbs free energies of 2,3,4,7,8-PeCDF decrease.

In addition, to investigate the influence of pressure on the adsorption of PeCDF on biochar, adsorption Gibbs free energies under different pressure were calculated. According to Fig. 6(b), whatever PeCDF molecule adsorbed on pristine, graphitic N, pyridinic N, or pyrrolic N doped biochar, the Gibbs adsorption energy keeps constant as the pressure increases from 0.25 Atm to 1.25 Atm. Pressure has been reported a significant influence on chemical adsorption and mass transfer (Wang et al., 2019; Zhou et al., 2018). Therefore, it is reasonable that pressure has no effect on the physical adsorption without a mass transfer barrier. Specially, the Gibbs free energies of 2,3,4,7,8-PeCDF before and after adsorption for different pressure were shown in Table S4. As the pressure increase, the Gibbs free energies of 2,3,4,7,8-PeCDF increase whatever PeCDF molecule adsorbed on pristine, graphitic N, pyridinic N, or pyrrolic N doped biochar.

4. Conclusion

In summary, the PeCDF adsorption mechanism on biochar with various nitrogen-containing functional groups has been systematically investigated by the DFT-D3 method. The results are as follows:

- (1) PeCDF molecule prefers to be adsorbed parallelly on the pristine and N-doped biochar and N doping promotes the PeCDF adsorption by enhancing π - π EDA interaction and electrostatic interaction.
- (2) Among various N doping biochar, pyrrolic N doping biochar presents the strongest interaction toward PeCDF molecule due to the highest adsorption energy and shortest interaction distance.
- (3) The effect of N doping species is more important than that of N doping content and the adsorption capacity of N doping biochar for PCDD/F can be improved by adding pyrrolic N group most efficiently.
- (4) The adsorption behavior of 2,3,4,7,8-PeCDF adsorbed on pyrrolic N and pyridinic N doped biochar results in the entropy increase of 2,3,4,7,8-PeCDF molecule, entropy decrease for graphitic N doped biochar.

The results reveal the PeCDF adsorption mechanism on biochar and guide the design of the efficient adsorption material for PCDD/F emission from industrial manufacture.

Credit author statement

Xiong, Shijian Xiong: Conceptualization, Methodology, Software, Data curation, Writing- Original draft. Minghui Tang: Writing-Reviewing and Investigation. Wenqian Jiang: Formal analysis. Jiamin Ding: Writing-Reviewing and Supervision. Juan Qiu: Formal analysis. Shengyong Lu: Formal analysis. Jianhua Yan: Writing-Reviewing and Supervision.

Declaration of competing interest

The authors declare no competing financial interest.

Data availability

Data will be made available on request.

Acknowledgment

This research is supported by the National Natural Science Foundation of China (No. 52006191), the Natural Science Foundation of Zhejiang Province (No. LY21E060007).

Appendix A. Supplementary data

Supplementary data to this article can be found online at <https://doi.org/10.1016/j.jenvman.2023.118611>.

References

- Atkinson, J.D., Hung, P.C., Zhang, Z., Chang, M.B., Yan, Z., Rood, M.J., 2015. Adsorption and destruction of PCDD/Fs using surface-functionalized activated carbons. *Chemosphere* 118, 136–142.
- Chang, Y.M., Hung, C.Y., Chen, J.H., Chang, C.T., Chen, C.H., 2009. Minimum feeding rate of activated carbon to control dioxin emissions from a large-scale municipal solid waste incinerator. *J. Hazard Mater.* 161, 1436–1443.
- Chen, T., Sun, C., Wang, T.J., Zhan, M.X., Li, X.D., Lu, S.Y., Yan, J.H., 2020. Removal of PCDD/Fs and CBzs by different air pollution control devices in MSWIs. *Aerosol Air Qual. Res.* 20, 2260–2272.
- Cheng, T., Bian, Y., Li, J., Ma, X., Yang, L., Zhou, L., Wu, H., 2023. Nitrogen-doped porous biochar for selective adsorption of toluene under humid conditions. *Fuel* 334, 126452.

- Enkovaara, J., Rostgaard, C., Mortensen, J.J., Chen, J., Dulak, M., Ferrighi, L., Gavnholt, J., Glinsvad, C., Haikola, V., Hansen, H.A., Kristoffersen, H.H., Kuisma, M., Larsen, A.H., Lehtovaara, L., Ljungberg, M., Lopez-Acevedo, O., Moses, P.G., Ojanen, J., Olsen, T., Petzold, V., Romero, N.A., Stausholm-Møller, J., Strange, M., Tritsarlis, G.A., Vanin, M., Walter, M., Hammer, B., Hakkinen, H., Madsen, G.K.H., Nieminen, R.M., Norskov, J., Puska, M., Rantala, T.T., Schiøtz, J., Thygesen, K.S., Jacobsen, K.W., 2010. Electronic structure calculations with GPAW: a real-space implementation of the projector augmented-wave method. *J. Phys. Condens. Mat.* 22.
- Fagan, S.B., Santos, E.J.G., Souza Filho, A.G., Mendes Filho, J., Fazzio, A., 2007. Ab initio study of 2,3,7,8-tetrachlorinated dibenzo-p-dioxin adsorption on single wall carbon nanotubes. *Chem. Phys. Lett.* 437, 79–82.
- Fang, Q.L., Zhu, B.Z., Sun, Y.L., Song, W.Y., Xu, M.G., 2020. Effects of Mn, Fe, and Ce doping on the adsorption property of gas molecules and oxidation of SO₂ on the NiO (100) surface. *Comput. Mater. Sci.* 180.
- Fu, J.-p., Xie, D.-p., Huang, J.-q., Yang, Y.-y., Feng, G.-x., Zhou, C.-f., Liao, H.-t., Qing, X., Zhang, M.-w., Wu, M.-l., Zhang, S.-k., 2022. Pollution level and regional migration of PCDD/fs in ambient air from pearl river delta, China. *Huanjing Kexue* 43, 2355–2362.
- Georgieva, I., Trendafilova, N., Dodoff, N., Kovacheva, D., 2017. DFT study of the molecular and crystal structure and vibrational analysis of cisplatin. *Spectrochim. Acta Part A: Molecular* 176, 58–66.
- Grimme, S., Antony, J., Ehrlich, S., Krieg, H., 2010. A consistent and accurate ab initio parametrization of density functional dispersion correction (DFT-D) for the 94 elements H-Pu. *J. Chem. Phys.* 132, 154104.
- Hafner, J., 2008. Ab-initio simulations of materials using VASP: density-functional theory and beyond. *J. Comput. Chem.* 29, 2044–2078.
- Hu, P., Wang, S., Zhuo, Y., 2021. CO₂ adsorption enhancement over Al/C-doped h-BN: a DFT study. *Chemosphere* 292, 133396.
- Huang, Y., Chen, Y., Li, Y., Zhou, L., Zhang, S., Wang, J., Du, W., Yang, J., Chen, L., Meng, W., Tao, S., Liu, M., 2022. Atmospheric emissions of PCDDs and PCDFs in China from 1960 to 2014. *J. Hazard Mater.* 424, 127320.
- Huang, X., Tang, M., Li, H., Wang, L., Lu, S., 2023. Adsorption of multicomponent VOCs on various biomass-derived hierarchical porous carbon: a study on adsorption mechanism and competitive effect. *Chemosphere* 313, 137513.
- Izadmehri, Z., Ganji, M.D., Ardjmand, M., 2017. Adsorption of 2, 3, 7, 8-tetrachlorodibenzo-p-dioxin (TCDD) on pristine, defected and Al-doped carbon nanotube: a dispersion corrected DFT study. *Vacuum* 136, 51–59.
- Jäger, R., Schneider, A.M., Behrens, P., Henkelmann, B., Schramm, K.W., Lenoir, D., 2004. Selective adsorption of polychlorinated dibenzo-p-dioxins and dibenzofurans by the zeolites UTD-1, SSZ-24, and ITQ-4. *Chem. Eur. J.* 10, 247–256.
- Kang, H.S., 2005. Theoretical study of binding of metal-doped graphene sheet and carbon nanotubes with dioxin. *J. Am. Chem. Soc.* 127, 9839–9843.
- Karademir, A., Bakoglu, M., Taspinar, F., Ayberk, S., 2004. Removal of PCDD/fs from flue gas by a fixed-bed activated carbon filter in a hazardous waste incinerator. *Environ. Sci. Technol.* 38, 1201–1207.
- Kasera, N., Kolar, P., Hall, S.G., 2022. Nitrogen-doped biochars as adsorbents for mitigation of heavy metals and organics from water: a review. *Biochar* 4.
- Kong, X.-k., Chen, Q.-w., 2013. Improved performance of graphene doped with pyridinic N for Li-ion battery: a density functional theory model. *Phys. Chem. Chem. Phys.* 15, 12982–12987.
- Kulkarni, P.S., Crespo, J.G., Afonso, C.A.M., 2008. Dioxins sources and current remediation technologies — a review. *Environ. Int.* 34, 139–153.
- Li, W., Lin, X., Yu, M., Mubeen, I., Buekens, A., Li, X., 2016. Experimental study on PCDD/Fs adsorption onto nano-graphite. *Aerosol Air Qual. Res.* 16, 3281–3289.
- Li, Y., Xing, B., Wang, X., Wang, K., Zhu, L., Wang, S., 2019. Nitrogen-doped hierarchical porous biochar derived from corn stalks for phenol-enhanced adsorption. *Energy Fuels* 33, 12459–12468.
- Liang, H., Wu, G., Zhang, H., Liu, Q., Yang, Q., Xiong, S., Yue, Y., Yuan, P., 2022. Controllable synthesis of N-doped hollow mesoporous carbon with tunable structures for enhanced toluene adsorption. *Separ. Purif. Technol.* 283, 120171.
- Lin, X., Huang, Q., Chen, T., Li, X., Lu, S., Wu, H., Yan, J., Zhou, M., Wang, H., 2014. PCDD/F and PCBz emissions during start-up and normal operation of a hazardous waste incinerator in China. *Aerosol Air Qual. Res.* 14, 1142–1151.
- Lin, Z., Wang, R., Tan, S., Zhang, K., Yin, Q., Zhao, Z., Gao, P., 2023. Nitrogen-doped hydrochar prepared by biomass and nitrogen-containing wastewater for dye adsorption: effect of nitrogen source in wastewater on the adsorption performance of hydrochar. *J. Environ. Manag.* 334, 117503.
- Liu, S., Wu, S., Cheng, H., 2023. Preparation and characterization of lignin-derived nitrogen-doped hierarchical porous carbon for excellent toluene adsorption performance. *Ind. Crop. Prod.* 192, 116120.
- Lu, S., Huang, X., Tang, M., Peng, Y., Wang, S., Makwarimba, C.P., 2021. Synthesis of N-doped hierarchical porous carbon with excellent toluene adsorption properties and its activation mechanism. *Environ. Pollut.* 284, 117113.
- Lv, Z.Y., Yu, Y., Ren, M., Dang, T., Wu, S., Zhou, H., Gao, L., Yue, J., Zhang, H., Jiping, C., 2021. Spraying polyacrylamide solution to improve the removal of particle-phase dioxins by bag filter in a full-scale municipal solid waste incineration system. *Chemosphere* 285, 131392.
- Ma, X., Li, L., Zeng, Z., Chen, R., Wang, C., Zhou, K., Su, C., Li, H., 2019. Synthesis of nitrogen-rich nanoporous carbon materials with C₃N-type from ZIF-8 for methanol adsorption. *Chem. Eng. J.* 363, 49–56.
- Momma, K., Izumi, F., 2011. VESTA 3 for three-dimensional visualization of crystal, volumetric and morphology data. *J. Appl. Crystallogr.* 44, 1272–1276.
- Ottaviani, M.F., Mazzeo, R., Turro, N.J., Lei, X., 2011. EPR study of the adsorption of dioxin vapours onto microporous carbons and mesoporous silica. *Microporous Mesoporous Mater.* 139, 179–188.

- Pan, W., Qi, Y., Wang, R., Han, Z., Zhang, D., Zhan, J., 2013. Adsorption of TCDD with 1-butyl-3-methylimidazolium dicyanamide ionic liquid: a combined molecular dynamics simulation and quantum chemistry study. *Chemosphere* 91, 157–164.
- Qian, Y.A., Posch, T., Schmidt, T.C., 2011. Sorption of polycyclic aromatic hydrocarbons (PAHs) on glass surfaces. *Chemosphere* 82, 859–865.
- Qiu, W., Dou, K., Zhou, Y., Huang, H., Chen, Y., Lu, H., 2018. Hierarchical pore structure of activated carbon fabricated by CO₂/microwave for volatile organic compounds adsorption. *Chin. J. Chem. Eng.* 26, 81–88.
- Qu, Z., Sun, F., Liu, X., Gao, J., Qie, Z., Zhao, G., 2018a. The effect of nitrogen-containing functional groups on SO₂ adsorption on carbon surface: enhanced physical adsorption interactions. *Surf. Sci.* 677, 78–82.
- Qu, Z.B., Sun, F., Liu, X., Gao, J.H., Qie, Z.P., Zhao, G.B., 2018b. The effect of nitrogen-containing functional groups on SO₂ adsorption on carbon surface: enhanced physical adsorption interactions. *Surf. Sci.* 677, 78–82.
- Ryu, J.Y., Mulholland, J.A., Kim, D.H., Takeuchi, M., 2005. Homologue and isomer patterns of polychlorinated dibenzo-p-dioxins and dibenzofurans from phenol precursors: comparison with municipal waste incinerator data. *Environ. Sci. Technol.* 39, 4398–4406.
- Schecter, A., 2013. *Dioxins and Health*. Springer Science & Business Media.
- Shen, Y., Zhang, N., 2019. Facile synthesis of porous carbons from silica-rich rice husk char for volatile organic compounds (VOCs) sorption. *Bioresour. Technol.* 282, 294–300.
- Tang, M., Huang, X., Peng, Y., Lu, S., 2020. Hierarchical porous carbon as a highly efficient adsorbent for toluene and benzene. *Fuel* 270, 117478.
- Wan, Z., Sun, Y., Tsang, D.C., Khan, E., Yip, A.C., Ng, Y.H., Rinklebe, J., Ok, Y.S., 2020. Customised fabrication of nitrogen-doped biochar for environmental and energy applications. *Chem. Eng. J.*, 126136.
- Wang, F., Sun, H., Ren, X., Zhang, K., 2017a. Sorption of naphthalene and its hydroxyl substitutes onto biochars in single-solute and bi-solute systems with propranolol as the co-solute. *Chem. Eng. J.* 326, 281–291.
- Wang, R., Zhang, D., Liu, C., 2017b. DFT study of the adsorption of 2,3,7,8-tetrachlorodibenzo-p-dioxin on pristine and Ni-doped boron nitride nanotubes. *Chemosphere* 168, 18–24.
- Wang, S., Feng, Q.H., Javadpour, F., Hu, Q.H., Wu, K.L., 2019. Competitive adsorption of methane and ethane in montmorillonite nanopores of shale at supercritical conditions: a grand canonical Monte Carlo simulation study. *Chem. Eng. J.* 355, 76–90.
- Wang, X., Guo, Z., Hu, Z., Ngo, H., Liang, S., Zhang, J., 2020. Adsorption of phenanthrene from aqueous solutions by biochar derived from an ammoniation-hydrothermal method. *Sci. Total Environ.* 733, 139267.
- Wang, V., Xu, N., Liu, J.C., Tang, G., Geng, W.T., 2021. VASPKIT: a user-friendly interface facilitating high-throughput computing and analysis using VASP code. *Comput. Phys. Commun.* 267.
- Wheeler, S.E., Bloom, J.W.G., 2014. Toward a more complete understanding of noncovalent interactions involving aromatic rings. *J. Phys. Chem. A* 118, 6133–6147.
- Yang, F., Sun, L., Xie, W., Jiang, Q., Gao, Y., Zhang, W., Zhang, Y., 2017. Nitrogen-functionalized biochars derived from wheat straws via molten salt synthesis: an efficient adsorbent for atrazine removal. *Sci. Total Environ.* 607–608, 1391–1399.
- Yang, W., Gao, Z., Liu, X., Ding, X., Yan, W., 2019. The adsorption characteristics of As₂O₃, PbO, PbO and PbCl₂ on single atom iron adsorbent with graphene-based substrates. *Chem. Eng. J.* 361, 304–313.
- Yang, Y., Qing, X., Xie, D., Chen, X., Zhang, S., Han, J., Liu, J., Fan, F., Jiang, W., 2022. Pollution characteristics and exposure risk assessment of PCDD/Fs in the ewaste dismantling region. *Acta Sci. Circumstantiae* 42, 441–449.
- Long, R.Q., Yang, R.T., 2001. Carbon nanotubes as superior sorbent for dioxin removal. *J. Am. Chem. Soc.* 123, 2058–2059.
- Zhan, M.X., Liu, Y.W., Ye, W.W., Chen, T., Jiao, W.T., 2021. Modification of activated carbon using urea to enhance the adsorption of dioxins. *Environ. Res.* 204, 112035.
- Zhang, H., He, W., Luo, X., Lin, X., Lu, X., 2014. Adsorption of 2,3,7,8-tetrachlorodibenzo-p-dioxins on intrinsic, defected, and Ti (N, Ag) doped graphene: a DFT study. *J. Mol. Model.* 20, 2238.
- Zhang, H.P., Hou, J.L., Wang, Y., Tang, P.P., Zhang, Y.P., Lin, X.Y., Liu, C., Tang, Y., 2017. Adsorption behavior of 2, 3, 7, 8-tetrachlorodibenzo-p-dioxin on pristine and doped black phosphorene: a DFT study. *Chemosphere* 185, 509–517.
- Zhang, C., Bai, L., Yao, Q., Li, J., Wang, H., Shen, L., Sippula, O., Yang, J., Zhao, J., Liu, J., Wang, B., 2022. Emission characteristics of polychlorinated dibenzo-p-dioxins and dibenzofurans from industrial combustion of biomass fuels. *Environ. Pollut.* 292.
- Zhang, L., Pei, Z., Lyu, B., Li, J., Zhao, Y., Wu, Y., 2023. Polychlorinated dibenzo-p-dioxins and dibenzofurans and dioxin-like polychlorinated biphenyls in human milk from national human breast milk monitoring in 2016–2019 in China. *Sci. Total Environ.* 872.
- Zhao, X., Li, X., Zhou, X., Chen, T., Lu, S., Cen, K., 2015. Modification of mesoporous activated carbon for adsorption of PCDD/Fs. *J. Zhejiang Univ. - Sci.* 49, 1842–1848.
- Zhou, X., Li, X., Xu, S., Zhao, X., Ni, M., Cen, K., 2015. Comparison of adsorption behavior of PCDD/Fs on carbon nanotubes and activated carbons in a bench-scale dioxin generating system. *Environ. Sci. Pollut. Control Ser.* 22, 10463–10470.
- Zhou, S.W., Xue, H.Q., Ning, Y., Guo, W., Zhang, Q., 2018. Experimental study of supercritical methane adsorption in Longmaxi shale: insights into the density of adsorbed methane. *Fuel* 211, 140–148.